Supporting Information

Synthesis of hypercrosslinked polymers spherical shell for highly effective cycloaddition of CO2 at ambient conditions

Shuqing Li, Zhen Zhan, Xiaoyan Wang*, Bien Tan*

*Key Laboratory of Material Chemistry for Energy Conversion and Storage, Ministry of Education, Hubei Key Laboratory of Material Chemistry and Service Failure, School of Chemistry and Chemical Engineering, Huazhong University of Science and Technology, Luoyu Road No. 1037, 430074, Wuhan (P. R. China)

E-mail: xiaoyan_wang@hust.edu.cn; bien.tan@mail.hust.edu.cn.

Chemicals. All chemicals and reagents were analytical grades or better and used without further purification. Tetraethyl orthosilicate (TEOS, 98%), ammonium hydroxide (NH_4OH, 28%), phenytrimethoxy-silane (PTMS), fluoranthene (FLA), N,N'-bis(salicylidene)ethylenediamine (Salen), triphenyl benzene (TPB), benzene (BEN), anhydrous aluminum chloride ($AlCl_3$), cobalt acetate tetrahydrate ($Co(OAc)_2 \cdot 4H_2O$), propylene oxide (PO), tetrabutylammonium bromide (TBAB), 1,2-dichloro-methane (DCM), anhydrous methanol, anhydrous ethanol, deionized water, tetrahydrofuran (THF), hydrofluoric acid (HF), propylene carbonate, 1,2-epoxybutane, buthylene carbonate, ethylene oxide, ethylene carbonate, 2-undecyloxirane, 4-undecy-1,3-dioxolan-2-one.

Characterization. Fourier transform infrared (FT-IR) spectra of solid samples were taken on Bruker Vertex 70 FT-IR spectrometer with the KBr disk method. Thermogravimetric analysis (TGA) was carried out on a PerkinElmer Instrument Puris 1 TGA and performed at room temperature to 800^{o}C in a nitrogen atmosphere with a heating rate of 10^{o}C min^{-1}. Scanning electron microscopy (SEM) images were taken on an FEI Sirion 200 field emission scanning electron microscope operated at 10 kV. Transmission electron microscopy (TEM) images were obtained from the Tecnai G2 F30 microscope (FEI Corp.). Gas (N_2, CO_2) sorption properties and specific surface area of samples were measured using a Micromeritics ASAP 2460 surface area and porosity analyzer. Samples were degassed at 120^{o}C for a minimum period of 8 h before analysis. Brunauer-Emmett-Teller (BET) surface areas were calculated from the linear part of the BET plot. Assuming the geometry of the slit, the Tarazona nonlocal density functional theory (NLDFT) model was used to calculate the pore size distribution through the N_2

adsorption isotherm. Total pore volumes (V_{toal}) were derived from nitrogen adsorption isotherm when the relative pressure P/P0=0.995. X-ray photoelectron spectroscopy (XPS) spectra were acquired using Krato AXIS-ULTRA DLD-600 photoelectron spectrograph. Inductively coupled plasma mass spectrometry (ICP) analysis was carried out on ICP-OES 730 (Agilent Corp. USA). The products of the CO_2 conversion reaction were identified by ^1H NMR spectra using a Bruker AV600 instrument in $CDCl_3$.

Figures

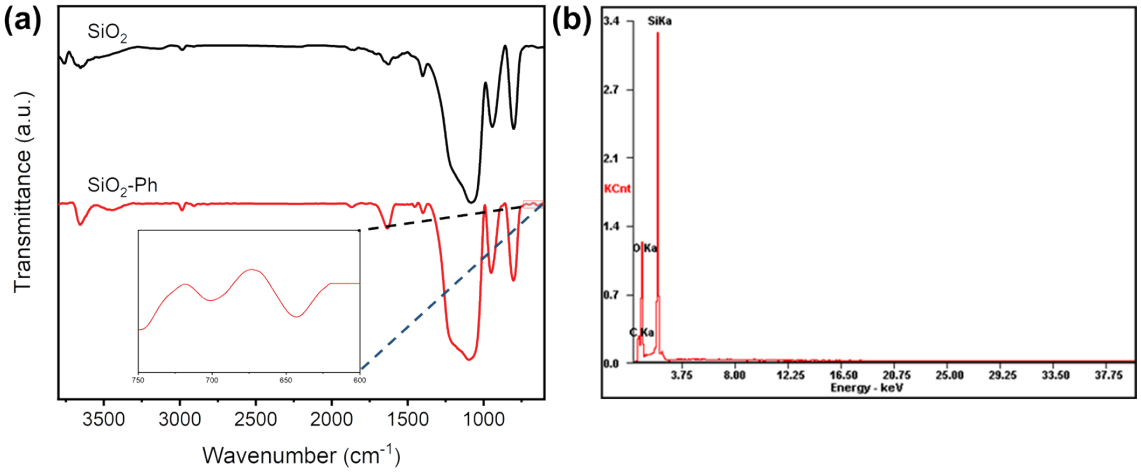

Figure S1 (a) FT-IR spectra of SiO_2 and SiO_2-Ph. (b) The Energy Dispersive Spectrometer (EDS) swept the spectrum graph of SiO_2-Ph.

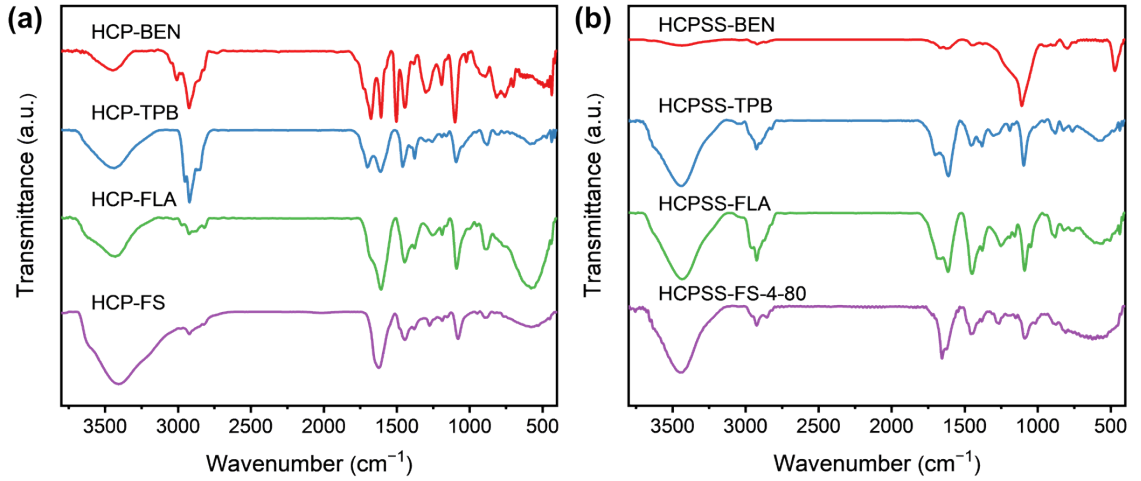

Figure S2 FT-IR spectra of (a) HCP-BEN, HCP-TPB, HCP-FLA and HCP-FS, (b) HCPSS-BEN, HCPSS-TPB, HCPSS-FLA and HCP-FS-4-80.

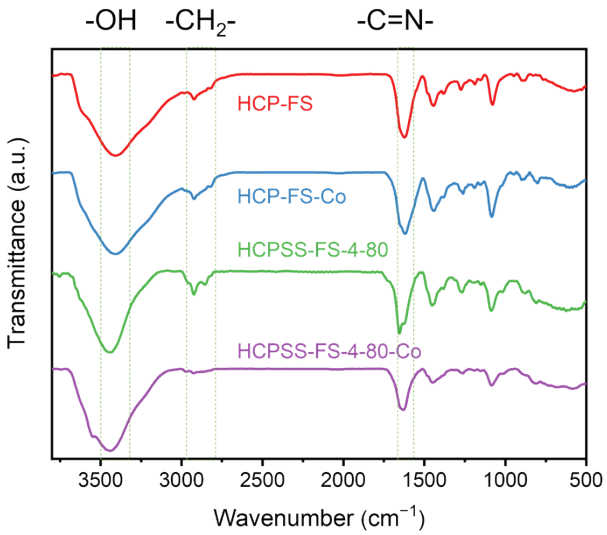

Figure S3 FT-IR spectra of HCP-FS, HCP-FS-Co, HCPSS-FS-4-80, HCPSS-FS-4-80-Co.

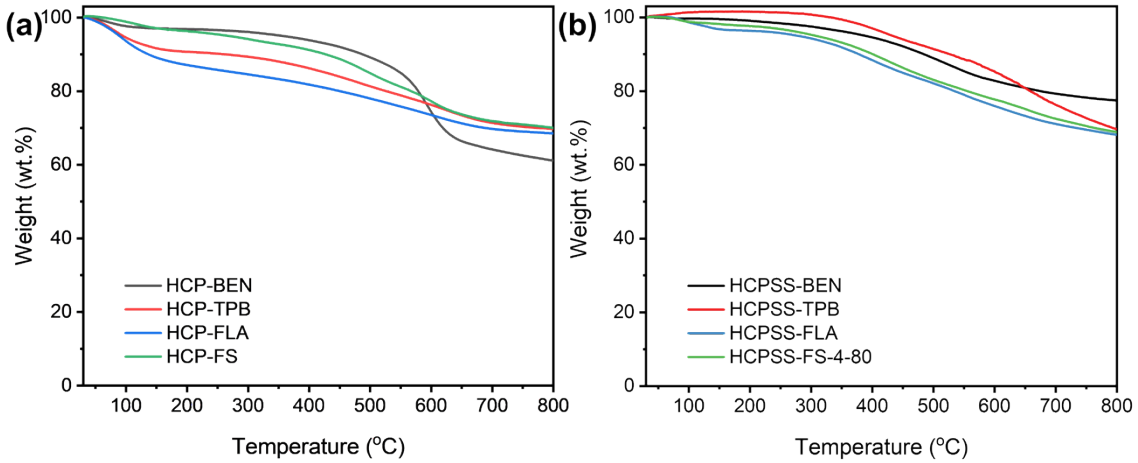

Figure S4 TGA of (a) HCP-BEN, HCP-PB, HCP-FLA and HCP-FS, (b) HCPSS-BEN, HCP-SS-TPB, HCPSS-FLA and HCPSS-FS-4-80 with a heating rate of 10°C min^{-1} (measured under N_2 atmosphere).

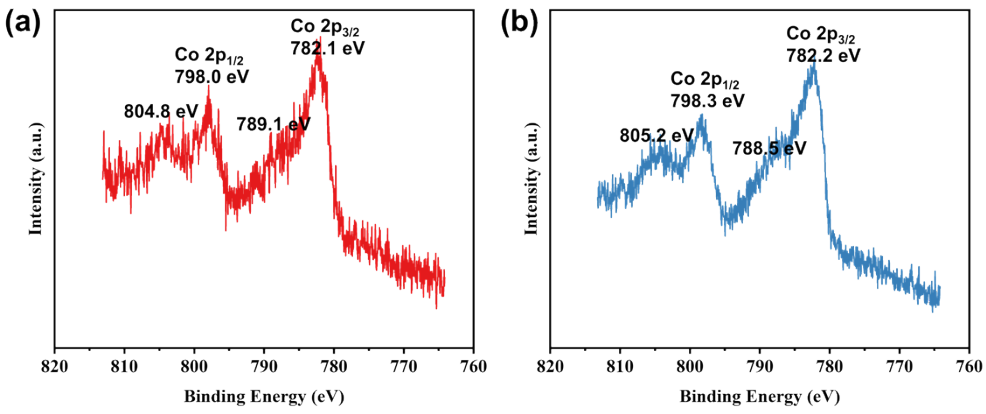

Figure S5 XPS spectra for Co 2p of (a) HCP-FS-Co, (b) HCPSS-FS-4-80-Co.

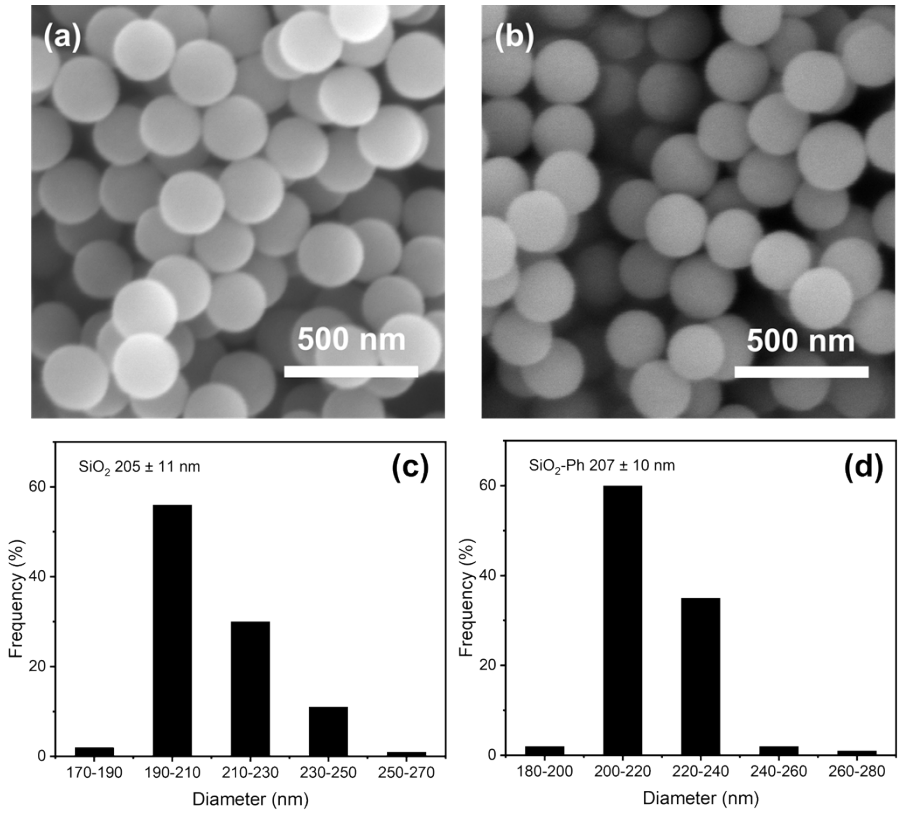

Figure S6 The SEM images of (a) SiO_2 and (b) SiO_2-Ph. The particle size distribution of (c) SiO_2, (d) SiO_2-Ph.

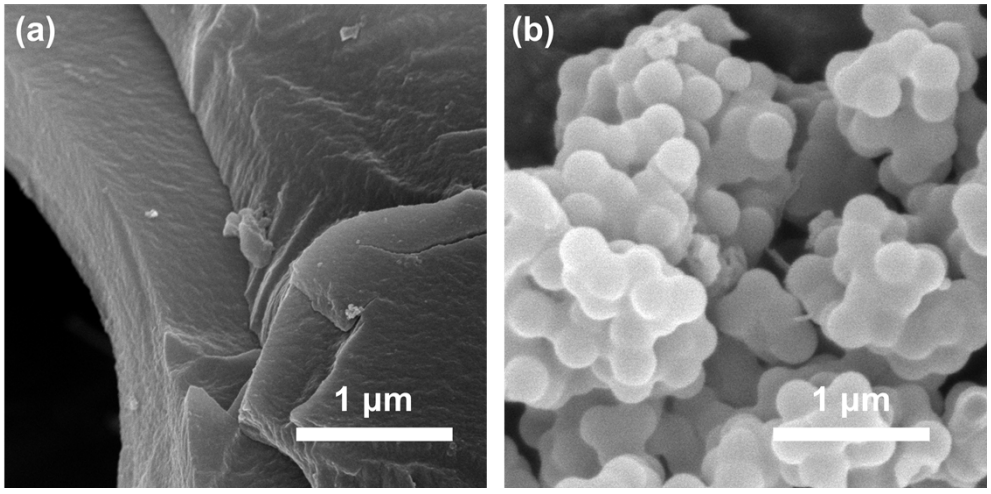

Figure S7 The SEM images of (a) HCP-FS and (b) HCPSS-FS-one-pot.

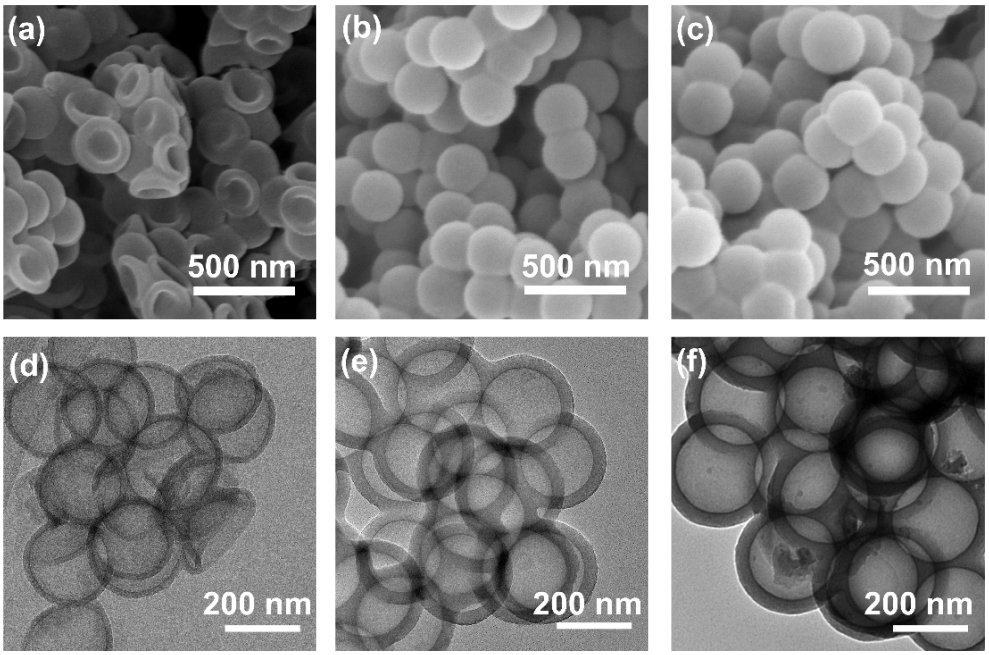

Figure S8 SEM images of (a) HCPSS-FS-5-80, (b) HCPSS-FS-4-80, (c) HCPSS-FS-3-80, TEM images of (d) HCPSS-FS-5-80, (e) HCPSS-FS-4-80, (f) HCPSS-FS-3-80.

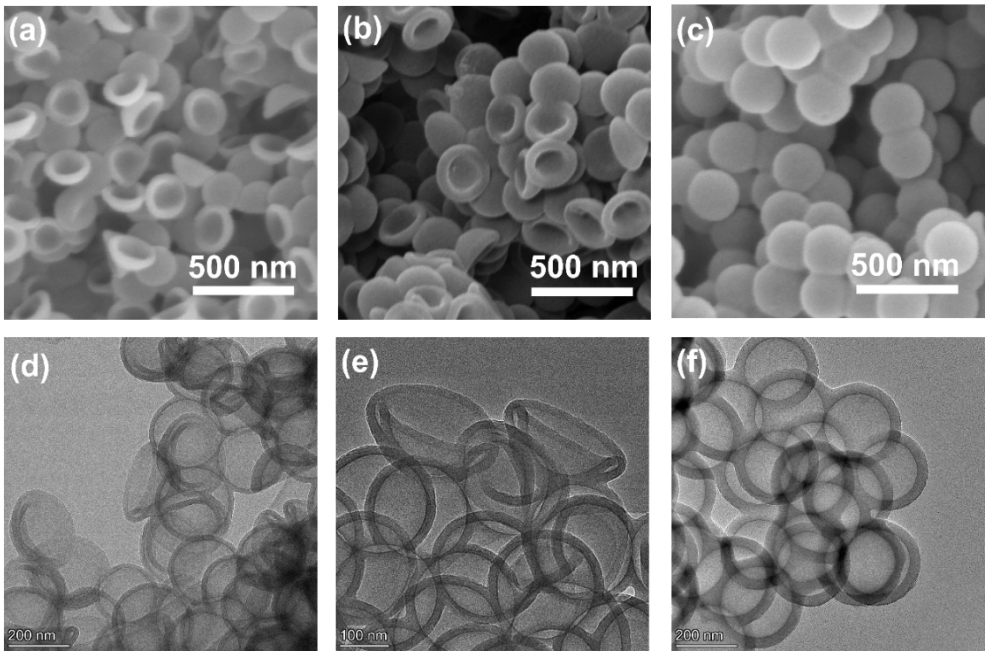

Figure S9 SEM images of (a) HCPSS-FS-4-30, (b) HCPSS-FS-4-40, (c) HCPSS-FS-4-80, TEM images of (d) HCPSS-FS-4-30, (e) HCPSS-FS-4-40, (f) HCPSS-FS-4-80.

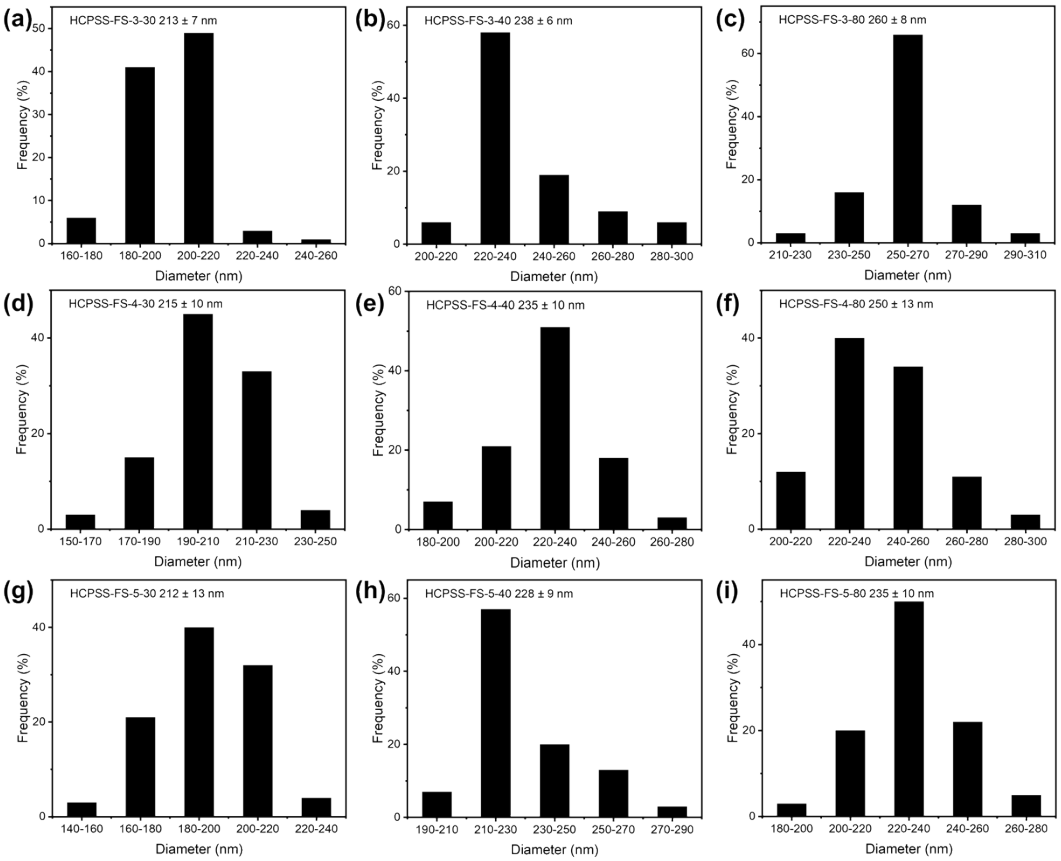

Figure S10 The particle size distribution of (a) HCPSS-FS-3-30, (b) HCPSS-3-40, (c) HCPSS-3-80, (d) HCPSS-FS-4-30, (e) HCPSS-FS-4-40, (f) HCPSS-FS-4-80, (g) HCPSS-5-30, (h) HCPSS-5-40, (i) HCPSS-5-80.

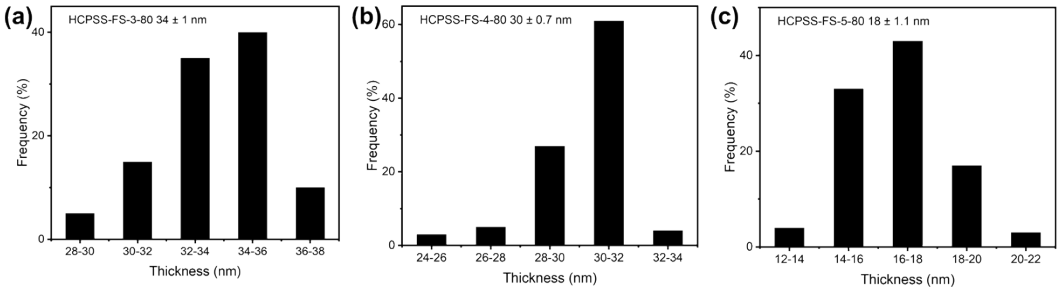

Figure S11 The thickness distribution of (a) HCPSS-FS-3-80, (b)HCPSS-FS-4-80, (c) HCPSS-FS-5-80.

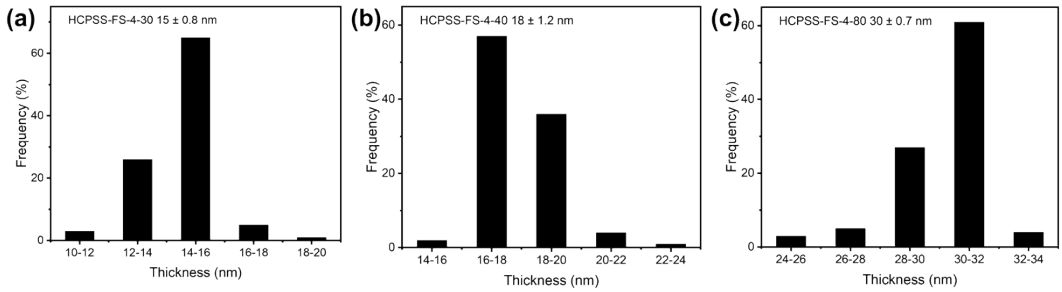

Figure S12 The thickness distribution of (a) HCPSS-FS-4-30, (b)HCPSS-FS-4-40, (c) HCPSS-FS-4-80.

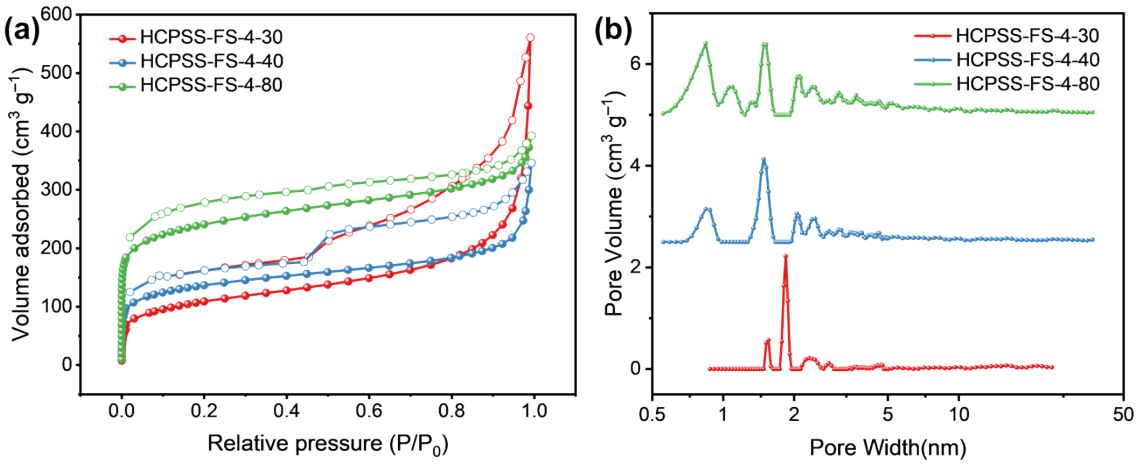

Figure S13 (a) N_2 sorption isotherms at 77 K and (b) pore size distributions of HCPSS-FS-4-30, HCPSS-FS-4-40, and HCPSS-FS-4-80.

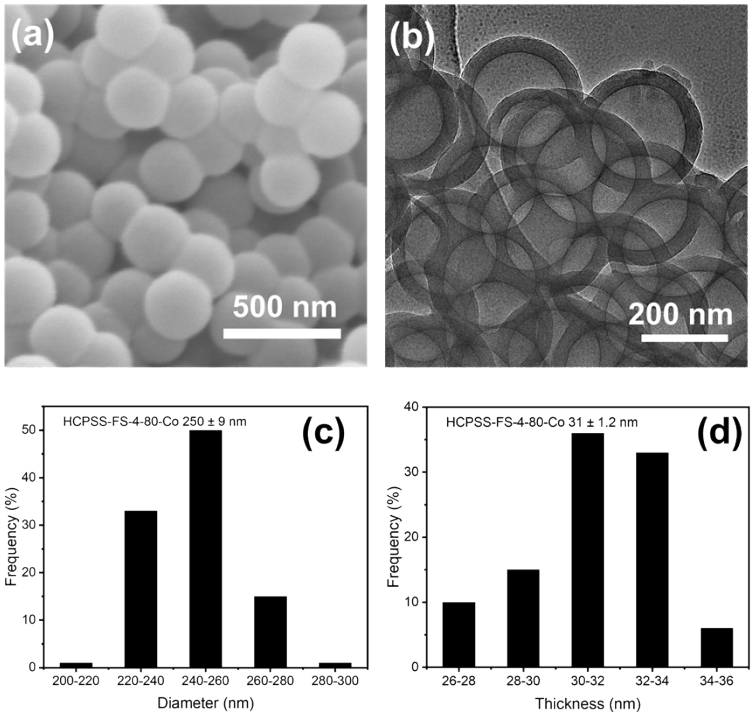

Figure S14 SEM images of (a) HCPSS-FS-4-80-Co and TEM images of (b) HCPSS-FS-4-80-Co. The particle size distribution of (c) HCPSS-FS-4-80-Co and the thickness distribution of (d) HCPSS-4-80-Co.

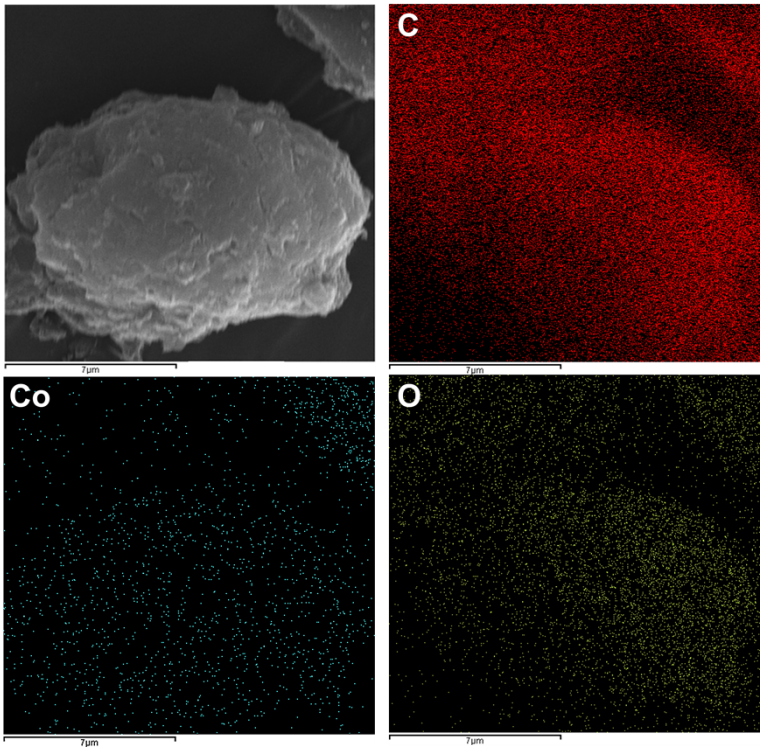

Figure S15 Electron image and element mapping (C, Co, and O) spectra for HCP-FS-Co.

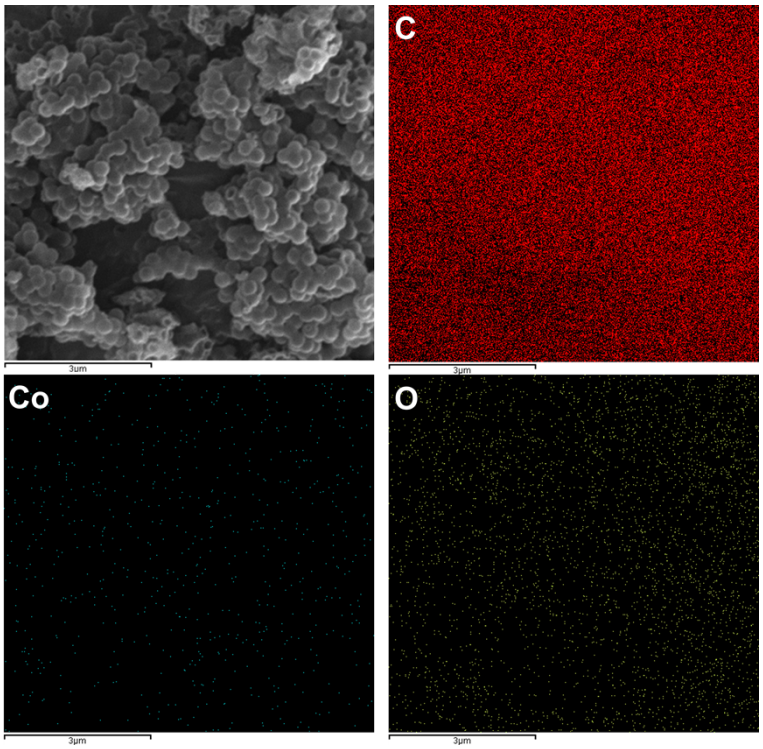

Figure S16 Electron image and element mapping (C, Co, and O) spectra for HCPSS-FS-4-80-Co

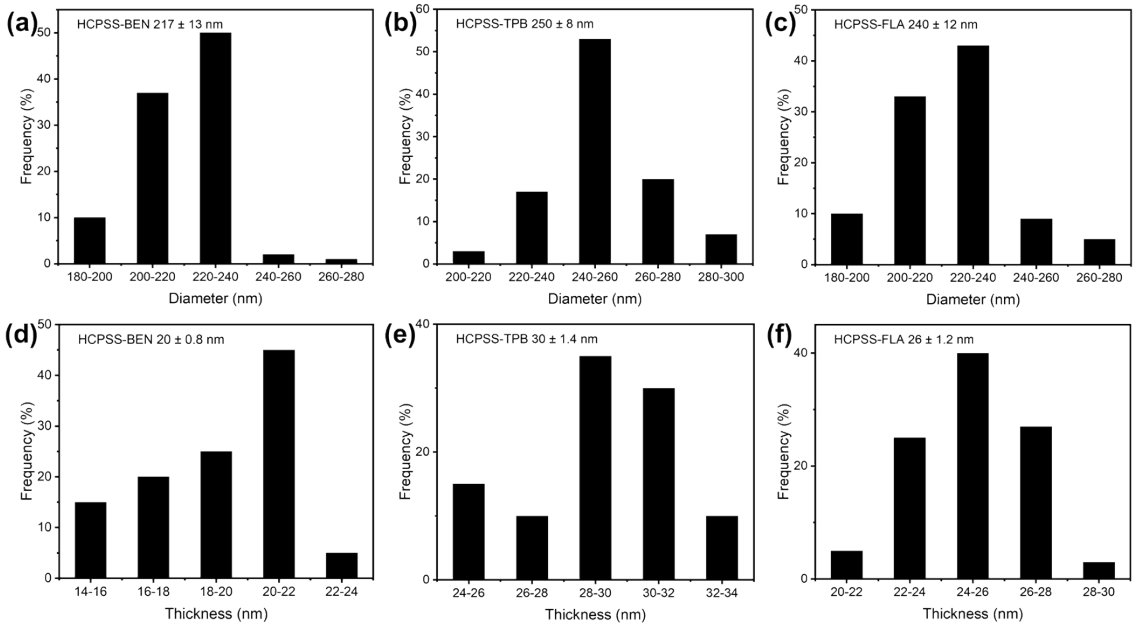

Figure S17 The particle size distribution of (a) HCPSS-BEN, (b) HCPSS-TPB, (c) HCPSS-FLA. The thickness distribution of (d) HCPSS-BEN, (e)HCPSS-TPB, (f) HCPSS-FLA.

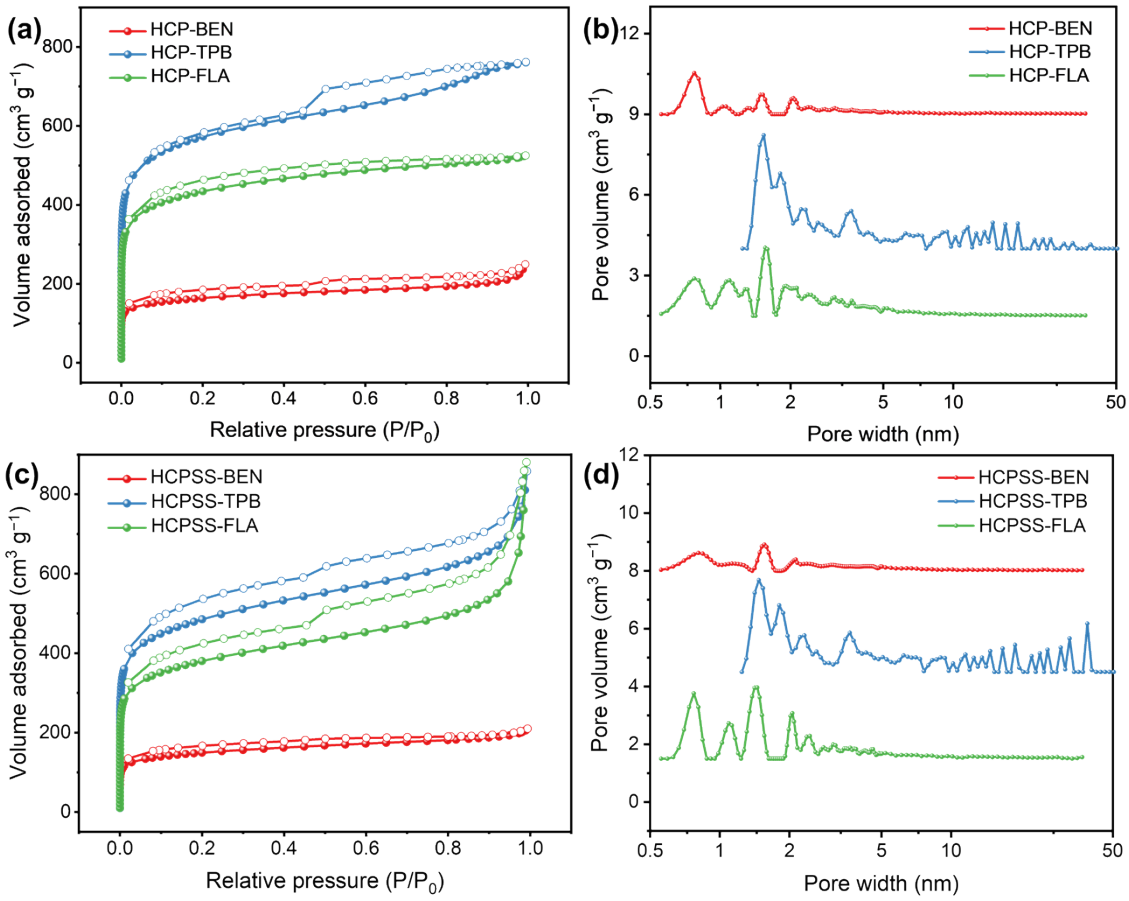

Figure S18 (a) N_2 sorption isotherms at 77 K and (b) pore size distributions calculated using DFT methods of HCP-BEN, HCP-TPB, and HCP-FLA. (c) N_2 sorption isotherms at 77 K and (d) pore size distributions calculated of HCPSS-BEN, HCPSS-TPB, and HCPSS-FLA.

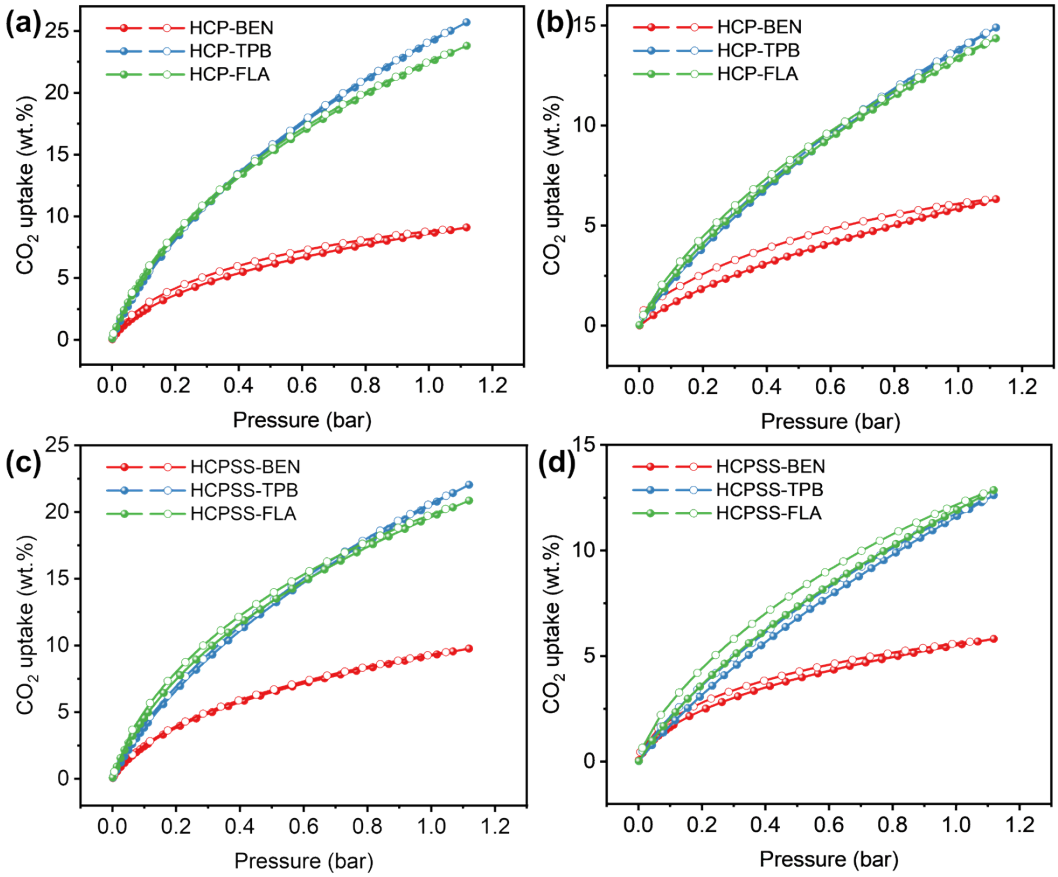

Figure S19 CO_2 adsorption and desorption isotherms of HCP-BEN, HCP-TPB and HCP-FLA at (a) 273 K and (b) 298 K. CO_2 adsorption and desorption isotherms of HCPSS-BEN, HCPSS-TPB and HCPSS-FLA at (c) 273 K and (d) 298 K.

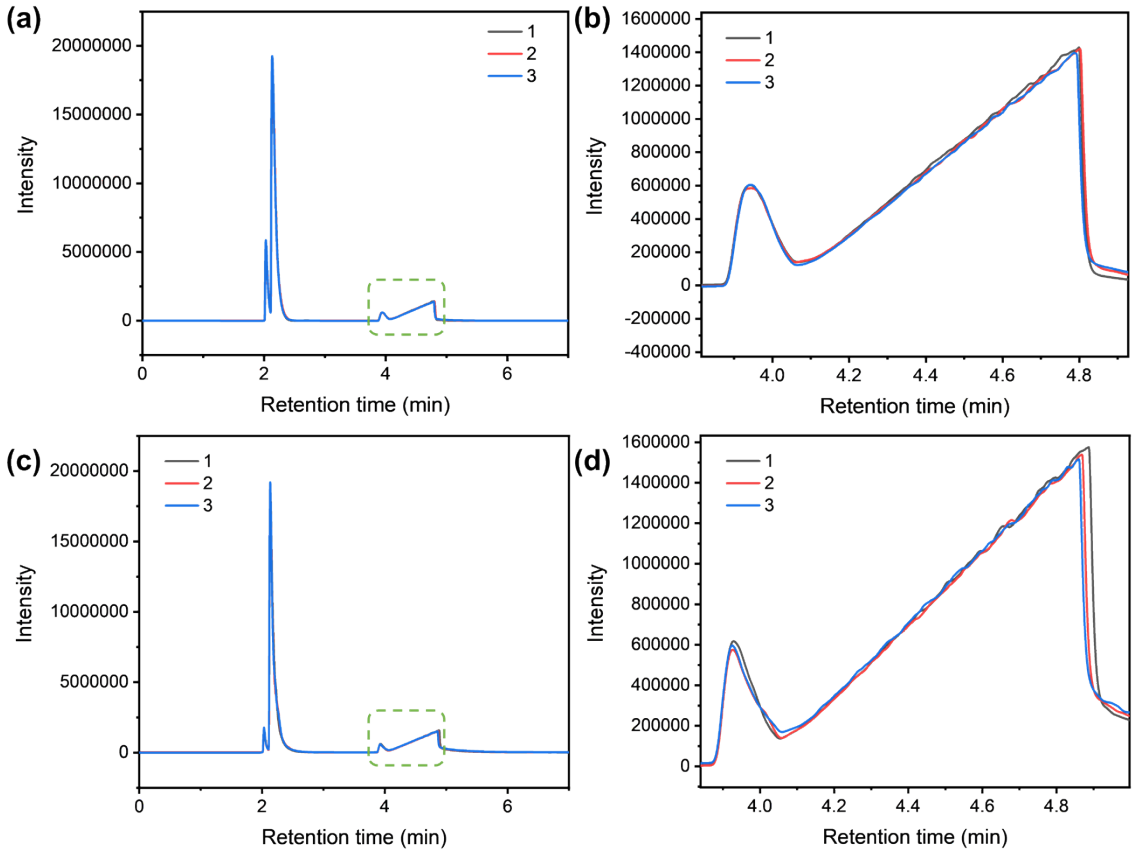

Figure S20 The GC spectrum of (a-b) HCP-FS-Co and (c-d) HCPSS-FS-4-80-Co. (Figures b and d are local enlarged views of the green dashed boxes of curves in figures a and c, respectively.)

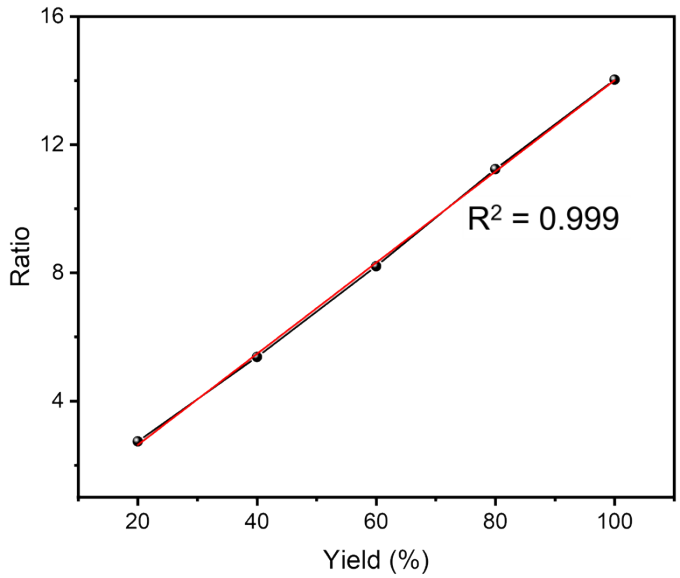

Figure S21 Linear fitting curve of internal standard and product peak-area ratio to yield (determined by GC).

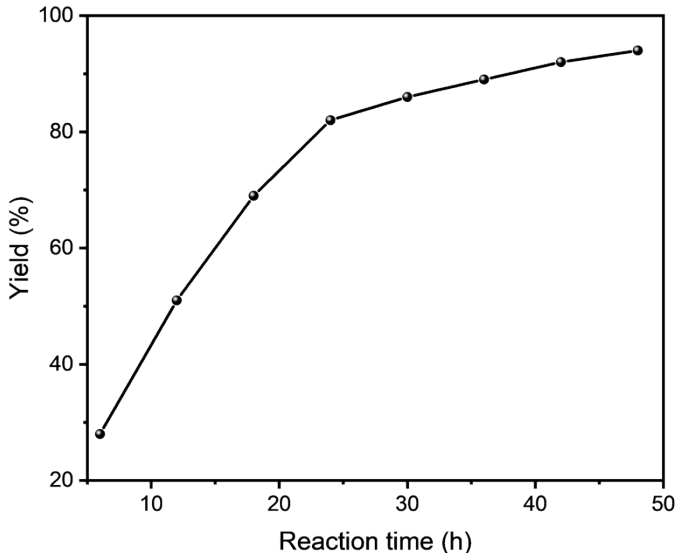

Figure S22 Effects of the reaction time on yield.

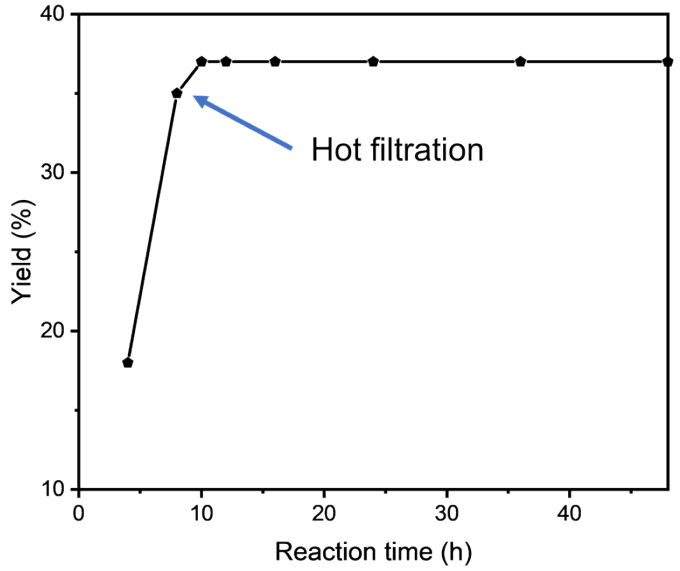

Figure S23 Hot filtration test. (Under the optimized reaction conditions, the reaction mixture was quickly divided into two parts by centrifugation after reaction for 8 h, and the upper clear liquid proceeded to react for another 40 h.)

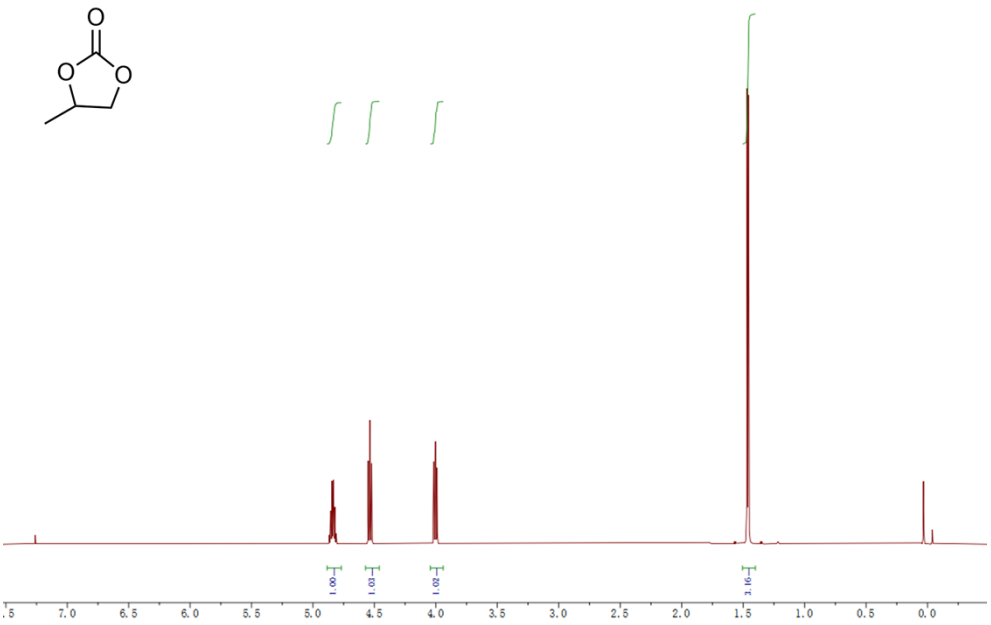

Figure S24 ^{1}H NMR images of propylene carbonate.

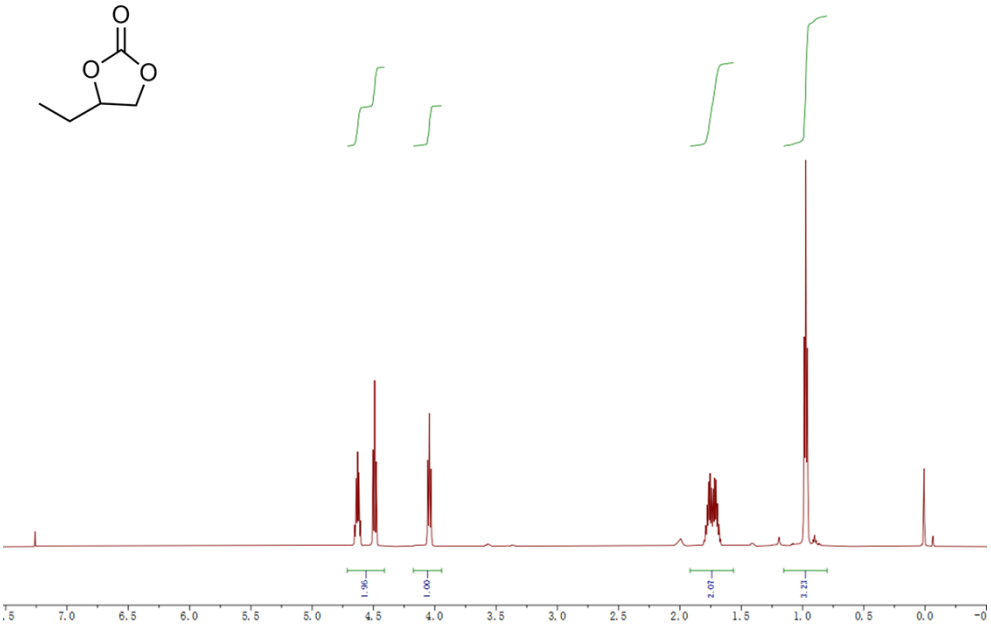

Figure S25 ^{1}H NMR images of buthylene carbonate.

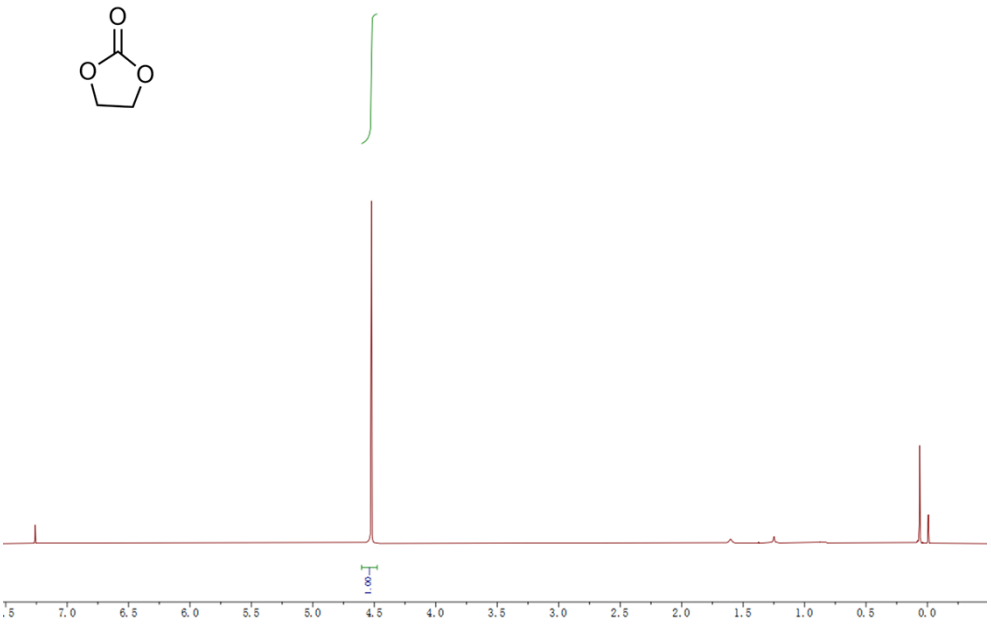

Figure S26 ^{1}H NMR images of ethylene carbonate.

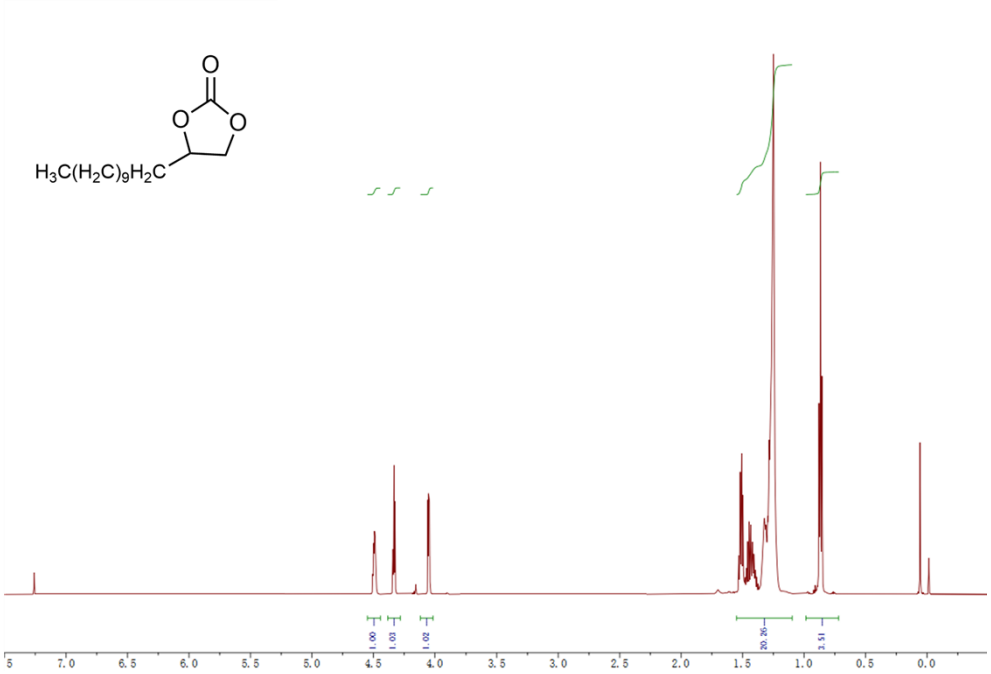

Figure S27 ^{1}H NMR images of 4-undecy-1,3-dioxolan-2-one.

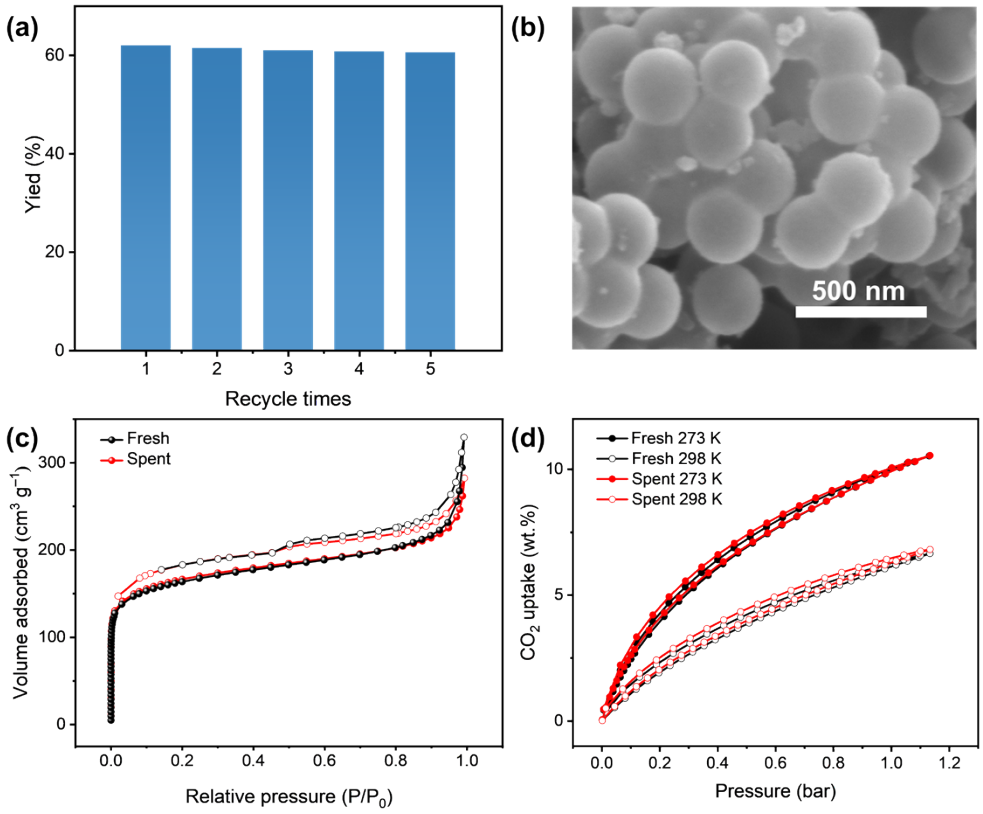

Figure S28 (a) The recycling experiments carried out at intermediate conversion. (b) The SEM image of spent HCPSS-FS-4-80-Co. (c) N_2 sorption isotherms at 77 K of the fresh and spent HCPSS-FS-4-80-Co. (d) CO_2 adsorption and desorption isotherms at 273 K and 298 K of the fresh and spent HCPSS-FS-4-80-Co.

Tables

Table S1 Elemental composition of samples.

Samples	C (wt.%)	H (wt.%)	N (wt.%)
HCP-FS	64.45	4.685	0.39
HCPSS-FS-4-80	81.40	5.120	0.40

Table S2 The Co content of the samples.

Samples	Co (wt.%)
HCP-FS-Co	3.41
HCPSS-FS-4-80-Co	3.30
HCPSS-FS-4-80-Co [a]	0.27

[a] Conditions: propylene oxide (50 mmol, 2.903 g), catalyst (HCPSS-FS-4-80-Co 40 mg, in which Co^{2+} 0.022 mmol, 1.32 mg), TBAB (2.4 mmol, 0.7737 g), 0.1 MPa CO_2, room temperature, after12 h reaction. The content of Co in supernatant was measured by ICP.

Table S3 Composition and porosity of the polymers.

Sample	S_{BET}[a] ($m^2\ g^{-1}$)	S_L[b] ($m^2\ g^{-1}$)	Pore Volume[c] ($cm^3\ g^{-1}$)	MPV[d] ($cm^3\ g^{-1}$)	CO_2 uptake (wt.%)[e]		CO_2 adsorption heat (kJ mol^{-1})
					273 K	298 K	
HCP-BEN	614	877	0.39	0.16	8.68	5.87	27.35
HCP-TPB	2135	3098	1.17	0.54	24.31	13.78	27.03
HCP-FLA	1616	2212	0.81	0.41	22.65	13.36	29.29
HCPSS-BEN	555	843	0.32	0.15	9.32	5.56	26.83
HCPSS-TPB	1790	2783	1.28	0.49	20.77	11.63	26.93
HCPSS-FLA	1403	2507	0.95	0.32	19.87	11.93	28.98

[a] Calculated from N_2 adsorption isotherms at 77 K using the BET model. [b] Calculated from N_2 adsorption isotherms at 77 K using the Langmuir equation. [c] Calculated from N_2 isotherms at 77 K and $P/P_0 = 0.995$. [d] Calculated from N_2 isotherm at $P/P_0 = 0.050$. [e] Adsorption capacity of CO_2 per gram at 273 K and 298 K (1 bar).

Table S4 Contrast with other materials

Entry	Substrate (mmol)	Co-catalyst	Co-catalyst /Substrate	P/T/t (MPa/°C/h)	Yield	Metal/ Metal-free	Ref.
1	50	TBAB	4.8%	0.1/25/48	94%	Metal	This work
2	20	TBAB	5.0%	3.0/120/2.5	85%	Metal	[1]
3	20	TPPB	5.0%	3.0/120/2.5	87%	Metal	[1]
4	20	DMAP	5.0%	3.0/120/2.5	72%	Metal	[1]
5	20	KI	5.0%	3.0/120/2.5	86%	Metal	[1]
6	1.43	$ZnBr_2$	0.9 wt.%	1.0/130/2.5	90%	Metal-free	[2]
7	1.43	-	-	1.0/120/4.0	78%	Metal-free	[3]
8	3	TBAB	2.0%	1.0/40/1.0	99%	Metal	[4]
9	10	TBAB	3.5%	0.1/29/48.0	99%	Metal	[5]
10	5	-	-	1.0/120/6.0	99%	Metal-free	[6]
11	160	-	-	3.0/140/2.0	90%	Metal, ILs	[7]
12	10	-	-	0.1/50/12.0	99%	ILs	[8]
13	5	-	-	0.1/80/60	96%	Metal, ILs	[9]
14	41.5	$ZnBr_2$	1.61 wt.%	2.0/100/3.0	97%	Metal, ILs	[10]
15	6.5	DMAP	1.0%	0.3/90/3.0	94%	Metal	[11]
16	2	-	-	0.1/60/60	99%	ILs	[12]
17	25	TBAB	4.8%	0.1/25/48	98%	Metal	[13]
18	15	-	-	1.0/120/2	90%	ILs	[14]
19[a]	20	-	-	3.0/120/4	81%	ILs	[15]
20	3	-	-	1.0/40/3	99%	Metal, ILs	[16]
21	4 wt.%	-	-	1.0/90/12	99%	Metal-free	[17]
22	25	TBAB	7.2%	0.1/25/48	95.4%	Metal	[18]
23	0.086	TBAB	1.43%	0.1/25/48	99%	Metal	[19]

[a] 15% CO_2+85% N_2

Table S5 The areas of the internal standard and product peaks obtained by GC.

Samples	Number of repeats	Internal standard peak area	Product peak area	Ratio	Yield (%)	Average yield (%)
HCP-FS-Co	1	4075375	35781196	8.78	62.88	63
	2	4105708	35408364	8.62	61.77	
	3	3985971	35047148	8.79	62.98	
HCPSS-FS-4-80-Co	1	3586871	47901392	13.35	94.75	94
	2	3636536	48642155	13.37	94.93	
	3	3716885	48162606	12.96	92.02	

References

1. A. Chen, Y. Zhang, J. Chen, L. Chen and Y. Yu, J. Mater. Chem. A, 2015, 3, 9807-9816.
2. Jinquan Wang, Jason Gan Wei Yang, G. Yi and Y. Zhang, Chem. Comm., 2015, 51, 15708-15711.
3. J. Wang, W. Sng, G. Yi and Y. Zhang, Chem. Comm., 2015, 51, 12076-12079.
4. Y. Chen, R. Luo, Q. Xu, W. Zhang, X. Zhou and H. Ji, ChemCatChem, 2017, 9, 767-773.
5. Z. Dai, Q. Sun, X. Liu, L. Guo, J. Li, S. Pan, C. Bian, L. Wang, X. Hu, X. Meng, L. Zhao, F. Deng and F. S. Xiao, ChemSusChem, 2017, 10, 1186-1192.
6. J. Li, D. Jia, Z. Guo, Y. Liu, Y. Lyu, Y. Zhou and J. Wang, Green Chem., 2017, 19, 2657-2686.
7. W. Wang, Y. Wang, C. Li, L. Yan, M. Jiang and Y. Ding, ACS Sustain. Chem. Eng., 2017, 5, 4523-4528.
8. Y. Xie, J. Liang, Y. Fu, M. Huang, X. Xu, H. Wang, S. Tu and J. Li, J. Mater. Chem. A, 2018, 6, 6660-6666.
9. J. Li, Y. Han, T. Ji, N. Wu, H. Lin, J. Jiang and J. Zhu, Ind. Eng. Chem. Res., 2019, 59, 676-684.
10. P. Puthiaraj, S. Ravi, K. Yu and W.-S. Ahn, Appl. Catal. B: Environmental, 2019, 251, 195-205.
11. M. M. Eva, V.-G. Antonio and I. Marta, Molecules, 2020, 25, 4598-4508.
12. Y. Zhang, K. Liu, L. Wu, H. Huang, Z. Xu, Z. Long, M. Tong, Y. Gu, Z. Qin and G. Chen, Dalton Tran., 2021, 50, 11878-11888.
13. H. Ouyang, K. Song, J. Du, Z. Zhan and B. Tan, Chem. Eng. J., 2021, 431, 134326.
14. D. Jia, L. Ma, Y. Wang, W. Zahng, J. Li, Y. Zhou, J. Wang. Chem. Eng. J., 2020, 390, 124652.
15. W. Zhang, F. Ma, L. Ma, Y. Zhou, J. Wang. ChemSusChem, 2020, 13, 341-350.
16. Y. Chen, R. Luo, Q. Xu, J. Jiang, X. Zhou, H. Ji. ChemSusChem, 2017, 10, 2534-2541.
17. O. Buyukcakir, S. H. Je, S. N. Talapaneni, D. Kim and A. Coskun, ACS Appl. Mater. Interfaces, 2017, 9, 7209-7216.
18. W. Y. Gao, Y. Chen, Y. Niu, K. Williams, L. Cash, P. J. Perez, L. Wojtas, J. Cai, Y. S. Chen and S. Ma, Angew. Chem. Int. Ed., 2014, 53, 2615-2619.
19. X. Zhang, H. Liu, P. An, Y. Shi, J. Han, Z. Yang, C. Long, J. Guo, S. Zhao, K. Zhao, H. Yin, L. Zheng, B. Zhang, X. Liu, L. Zhang, G. Li, Z. Tang, Sci. Adv., 2020, 6, eaaz4824.